Probing the Folding Transition State of Ubiquitin Mutants by Temperature-Jump-Induced Downhill Unfolding[†]

Hoi Sung Chung,[‡] Ali Shandiz,[§] Tobin R. Sosnick,[§] and Andrei Tokmakoff*[,‡]

Department of Chemistry, Massachusetts Institute of Technology, Cambridge, Massachusetts 02139, and Department of Biochemistry and Molecular Biology, Institute for Biophysical Dynamics, The University of Chicago, Chicago, Illinois 60637

Received August 25, 2008; Revised Manuscript Received October 25, 2008

ABSTRACT: Crucial to revealing mechanistic details of protein folding is a characterization of the transition state ensemble and its structural dynamics. To probe the transition state of ubiquitin thermal unfolding, we examine unfolding dynamics and kinetics of wild-type and mutant ubiquitin using time-resolved nonlinear infrared spectroscopy after a nanosecond temperature jump. We observe spectral changes on two different time scales. A fast nonexponential microsecond phase is attributed to downhill unfolding from the transition state region, which is induced by a shift of the barrier due to the rapid temperature change. Slow millisecond changes arise from thermally activated folding and unfolding kinetics. Mutants that stabilize or destabilize β strands III−V lead to a decreased or increased amplitude of the microsecond phase, indicating that the disruption or weakening of these strands occurs in the transition state. Unfolding features from microseconds to milliseconds can be explained by temperature-dependent changes of a two-dimensional free energy surface constructed by the native contacts between β strands of the protein. In addition, the results support the possibility of an intermediate state in thermal unfolding.

One of the most striking features in protein folding is its cooperativity. Many small proteins consisting of fewer than 100 residues show a single-step folding transition (*1*−*3*), which can be described by simple thermally activated two-state chemical kinetics. In this picture, folding and unfolding can be understood by characterizing the folded and unfolded states, and the transition state between them. A characterization of the transition state is at the heart of describing the folding dynamics, the time evolution of the protein structure, and the mechanistic details of folding.

Unfortunately, the short lifetime and small population prevent a direct observation of the transition state. Alternate strategies for characterizing the transition state involve understanding how the manipulation of microscopic variables influences the free energy surface. Of these approaches, ϕ analysis has been most widely used to map the transition state (*4, 5*). In this method, the effect of a given point mutation can be quantified by the ratio of the free energy change of the transition state to that of the folded state (ϕ value). A series of point mutations is used to deduce the involvement of each residue in the transition state. As a complementary method, ψ analysis has been developed, which is useful for investigating the role of pairwise contacts in the folding transition state (*6*−*8*). In this method, two histidine mutations (bi-His) are introduced in such a way that the two mutated residues can coordinate a metal ion. The stability of the bound residues can be controlled continuously by varying the concentration of divalent metal ions. This method has proven effective for stabilizing two β strands or a turn of an α helix.

Both ϕ and ψ analyses are indirect ways of mapping the transition state. Direct dynamic information about the transition state is hidden under the larger changes of the folded and unfolded state. An alternative approach is to observe the folding or unfolding dynamics directly using downhill folders for which no barrier to folding exists (*9, 10*). Many small proteins, of which folding rates are close to the "folding speed limit" (*11*), show global (*12, 13*) or conditional downhill unfolding features (*14*), although some of the interpretations of these results remain controversial (*15*−*17*).

Ubiquitin is a 76-residue protein consisting of one α helix and five β strands (Figure 1a), with folding behavior often interpreted in the context of two-state kinetics. However, several observations suggest a deviation from the simple two-state picture depending on experimental conditions. In spite of its small size, ubiquitin is divided into stable and less stable regions. A fragment study has reported that the N-terminal peptides (residues 1−35) show a small population having a nativelike structure, while C-terminal peptides (residues 36−76) form a nonnative structure (*18, 19*). Also, a partially folded structure of ubiquitin, including strands I and II and the α helix, has been observed in the organic solvent and water mixture (*20*−*22*). The ϕ analysis has described the transition state of ubiquitin folding as being localized in the β hairpin (strands I and II) and the α helix (*23*), a conclusion supported by molecular dynamics simulations (*24*). The extension of the transition state to strands V and III has been reported using ψ value analysis (*7, 8*). In spite of these issues, all of these results suggest a sequential

[†] This work was supported by a grant from the National Science Foundation (CHE-0616575, A.T.) and the National Institutes of Health (GM55694, T.R.S.).

* To whom correspondence should be addressed. Phone: (617) 253-4503. Fax: (617) 253-7030. E-mail: tokmakof@mit.edu.

[‡] Massachusetts Institute of Technology.

[§] The University of Chicago.

10.1021/bi801603e CCC: $40.75
Published on Web 12/03/2008

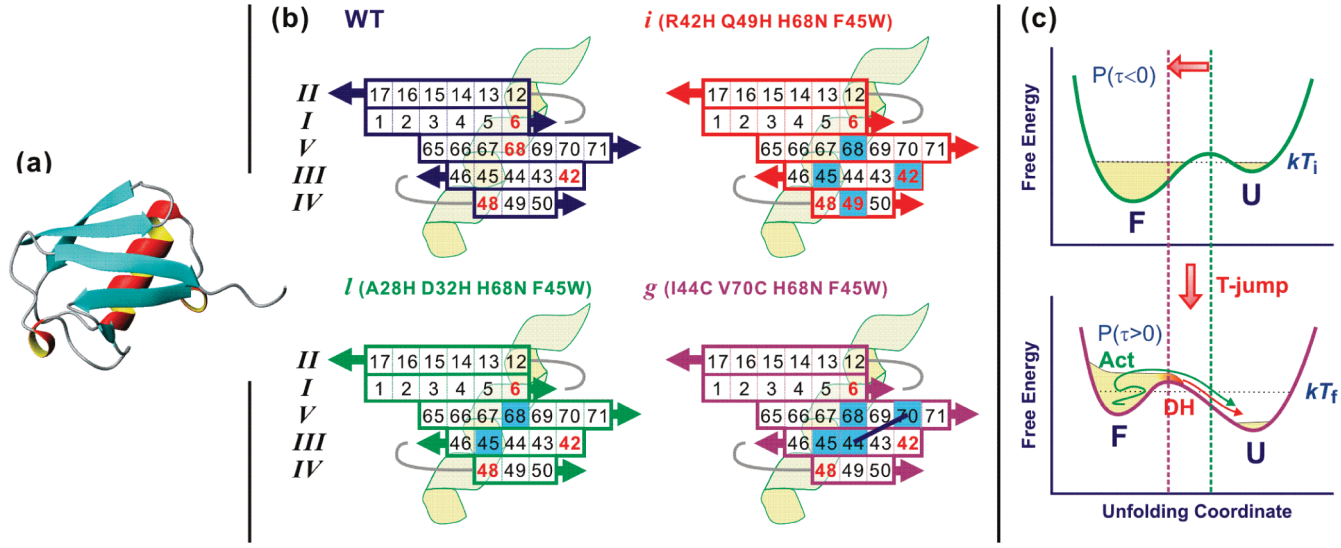

FIGURE 1: Structure of ubiquitin, mutations, and T-jump experiment. (a) Crystal structure of wild-type ubiquitin composed of five β strands and one α helix [Protein Data Bank (PDB) entry 1UBQ] (*50*). (b) Projection of the β sheet registry of ubiquitin. Amino acid residue numbers are indicated in the β sheet. Positively charged residues are marked with red numbers. Mutated residues are indicated with blue-filled square boxes. For mutant *l*, there are two more mutations at residues 28 and 32 located in the C-terminus (top right part) of the α helix, which are not shown. Residues 44 and 70 in mutant *g* are covalently linked, as shown with black lines. (c) A T-jump not only changes the relative stability of the folded and unfolded state but also induces a barrier shift toward the folded state. The latter prepares a small population near the barrier (transition state) that shows nonexponential relaxation (downhill unfolding, DH), and the former appears as millisecond activated unfolding (Act).

folding scenario in which folding of the N-terminal β hairpin and helix is followed by folding of the rest of the protein.

The ability to observe sequential folding or unfolding dynamics of ubiquitin would benefit from fast initiation and detection methods. A nanosecond temperature-jump (T-jump)[1] technique has been used to follow a time evolution of the species from the transition state. The experimental concept is illustrated in Figure 1c. A rapid T-jump induces a shift of the free energy barrier toward the folded well according to the Hammond postulate (*25*), positioning a small folded population near the barrier (A). This subensemble unfolds in a downhill manner. Unfolding of this species is temporally isolated (microseconds) from the main unfolding phase (milliseconds) and provides direct information about the unfolding dynamics. The unfolding dynamics of ubiquitin's β sheet has been probed using this rapid initiation followed by a structure-sensitive nonlinear infrared probe such as dispersed vibrational echo (DVE) (*26*) and two-dimensional infrared (2D IR) spectroscopy (*27*). Like other experimental observations, these studies supported a sequential folding−unfolding scenario in that unfolding of less stable strands III−V precedes unfolding of stable strands I and II (see Figure 1b). Sequential unfolding has also been observed in the high-temperature unfolding simulation (*28*). On the basis of these results, a two-dimensional free energy surface was proposed and calculated (*29*). This free energy surface consists of two reaction coordinates, the number of native contacts between stable strands I and II and among less stable strands III−V. Finally, a temperature-dependent T-jump study has suggested an increased heterogeneity of the transition state at high temperatures, namely multiple unfolding routes (*30*).

[1] Abbreviations: DVE, dispersed vibrational echo; T-jump, temperature jump; SVD, singular-value decomposition; 2D IR, two-dimensional infrared; WT, wild-type.

In this paper, we report dispersed vibrational echo (DVE)-probed T-jump experiments with the aim of improving our understanding of the transition state and unfolding dynamics of ubiquitin. Three ubiquitin mutants are investigated. Two mutants have bihistidine substitutions either in the helix (mutant *l*, residues 28 and 32) or across β strands III and IV (mutant *i*, residues 42 and 49) (*7*). A third, bicysteine mutant (*g*, residues 44 and 70) uses a stabilizing synthetic cross-link across strands III and V (*31*). The change in the downhill unfolding amplitude that occurs with destabilization or stabilization of strands III−V reveals the involvement of these strands in the transition state. The microsecond downhill unfolding and millisecond barrier crossing are described in the picture of the two-dimensional free energy surface. The increased and decreased downhill unfolding amplitudes of mutants *i* and *g* support the presence of an intermediate state on the native side of the rate-limiting barrier.

MATERIALS AND METHODS

Materials. Wild-type ubiquitin (WT) was purchased from Sigma-Aldrich (U6253) and used without further purification. We use three of an extensive series of mutants that have been cloned in the studies of ubiquitin folding (*7, 8, 31*). These mutants, named *i*, *l*, and *g*, have the following substitutions: *i*, R42H, Q49H, H68N, and F45W; *l*, A28H, D32H, H68N, and F45W; and *g*, I44C, V70C, H68N, and F45W. To remove a trace of trifluoroacetic acid (TFA) added in the purification step, mutant samples were lyophilized under acidic conditions (0.18% DCl in D_2O). Approximately 5 mg of each mutant sample was lyophilized twice more after being dissolved in 500−800 mL of D_2O. The experiment was performed at a sample concentration of 30 mg/mL in the 0.35% DCl solution. The solution is loaded between two 1 mm thick CaF_2 windows separated by a 50 μm thick Teflon spacer, which is mounted on a temperature-

controlled brass cell. The temperature is controlled within 0.1 °C by water circulation.

The experiments were performed under acidic conditions for reversible thermal unfolding. Therefore, all side chain amine groups, indicated by red numbers in Figure 1b, are positively charged. In WT, there are five positively charged residues in the β sheet. Since the side chains of Lys6, Arg42, and His68 are oriented outward from the hydrophobic core, while those of Lys11 and Lys48 penetrate inward, the repulsion between the side chains of strands I and II (Lys6−Lys11) and III and IV (Arg42−Lys48) would presumably be small and would not affect the stability of proteins. However, the repulsion among residues 6, 68, and 42, the side chains of which are on the same side, destabilizes the protein and lowers the melting temperature relative to neutral pH (*32, 33*).

Three different mutants are named according to the convention in refs *7* and *31*. The locations of mutated residues are shown with blue-colored boxes in the projected β sheet in Figure 1b. Mutants *i* and *l* are bi-His mutants of the β sheet and α helix, respectively, which were originally designed for ψ analysis (*7*). However, we cannot utilize the metal ion-induced ligation of the mutated residues because the pH is lower than the pK_a of His (6.5). Under this condition, required for reversible unfolding, the side chain of the His residue is protonated and cannot bind to the metal ion. Instead, the mutation affects the protein stability by charge−charge repulsion and disruption of structure-stabilizing hydrogen bonding networks for the water in the vicinity of those residues. In all mutants, Phe45 was mutated to Trp to allow fluorescence detection and His68 is mutated to Gln to avoid an unwanted metal ion-induced linkage in the original ψ value analysis experiments (*7, 8*). The Trp mutation at residue 45 is known to destabilize the protein slightly by ~0.4 kcal/mol (*34*). On the other hand, removal of the charged His68 stabilizes the protein.

Mutant *g* differs from mutants *i* and *l* in that the β sheet is stabilized through a covalent linkage. In this mutant, residues 44 and 70 in strands III and V are mutated to Cys and then cross-linked with dichloroacetone to form a covalent -S-CH_2-CO-CH_2-S- bridge (*31*). Therefore, the stability of strands III and V is greatly increased. Control experiments with the unlinked bi-Cys mutant with excess dithiothreitol (DTT) were attempted; however, thermal aggregation occurred too rapidly at 58 °C (near the melting temperature) for meaningful data to be obtained. A quoted "mutant *g*" indicates the covalently linked version in this paper.

Equilibrium and transient data of WT were adopted from our previous study (*30*) for comparison with those of mutants.

Amide I Vibrational Spectroscopy. Amide I vibrational spectroscopy has been used extensively in protein folding research because of its spectral isolation from most side chain vibrations and its sensitivity to the protein secondary structures (*35*). Amide I vibration is primarily a carbonyl stretching of the peptide backbone, but characteristic collective modes are formed by electrostatic couplings according to the symmetries of secondary structures. These couplings induce a big splitting between two vibrations of the antiparallel β sheet, $\nu_\perp$ and $\nu_\parallel$ modes located at <1650 and >1680 cm^{-1}, respectively. The intensity and the position (or red shift) of the $\nu_\perp$ mode reflect the size of the β sheet and report on the number of β strands in contact (*36*). The $\nu_\parallel$ mode is insensitive to the size of the β sheet, but it provides the evidence of the presence of at least two β strands, the β hairpin. Vibrations of the α helix are also composed of *A* and E_1 vibrations, but the two modes are not resolved due to the small splitting compared to the wide intrinsic line width of the infrared spectrum. Also, vibrations of the random coil component overlap spectrally with the α helical peak. Empirical assignments of the α helical and random coil vibrations are 1640 and 1650 cm^{-1}, respectively (*37*). In this paper, we will focus on the β sheet vibrations, especially the $\nu_\perp$ mode.

Nonlinear Infrared Spectroscopy. Thermal unfolding of proteins was monitored by DVE spectroscopy (*38, 39*). Three temporally coincident femtosecond pulses (90 fs in fwhm; $\lambda = 6$ μm) are focused on the sample (100 μm diameter), and the emitted third-order nonlinear signal is dispersed onto the liquid nitrogen-cooled HgCdTe (MCT) array detector by a monochromator. The DVE spectrum is a one-dimensional projection of the 2D IR spectrum, which monitors couplings between vibrations by cross-peak formation. Recently, transient 2D IR spectroscopy has been reported (*27, 40*), but we performed transient DVE spectroscopy in this paper due to the fast aggregation of mutant ubiquitin. In spite of its one-dimensional nature, DVE spectroscopy differs from FTIR because of its sensitivity to vibrational couplings and has been used to examine the equilibrium and transient thermal unfolding of proteins and peptides (*26, 39, 41*). Experimental details of ultrafast nonlinear IR spectroscopy have been described elsewhere (*38*).

Laser Temperature Jump. The laser T-jump has been widely used to monitor fast folding−unfolding kinetics of various proteins and peptides (*9, 10, 41−43*). In this paper, approximately 10 °C was jumped from the temperature near the melting points of proteins. A 5 mJ, 7 ns T-jump laser pulse ($\lambda = 2$ μm) is generated from a BBO-based optical parametric oscillator (OPO) pumped by a frequency-doubled Q-switched Nd:YAG laser. A T-jump pulse is focused (500 μm diameter) and overlapped with probe (6 μm) pulses. The pulse excites the first overtone of the D_2O solvent's O−D stretching vibration, and subsequent picosecond vibrational relaxation results in the temperature rise on the same time scale of the T-jump pulse duration of 7 ns. A fine delay τ between the T-jump pulse and the first probe pulse is controlled by an electronic delay generator with an accuracy of 2 ns. Since the T-jump laser and the 6 μm femtosecond probe are run by 20 Hz and 1 kHz, respectively, 50 pulses can probe spectral changes from τ to 49 ms + τ with a 1 ms interval after a T-jump. Details of the T-jump experiments, including delay controls, have been reported elsewhere (*40*).

RESULTS

Equilibrium Thermal Unfolding. The representative equilibrium thermal unfolding of ubiquitins monitored through their DVE spectra is shown with melting curves in Figure 2. Temperature-dependent spectra of WT and three mutants are similar, though only DVE spectra of mutant *i* are shown in Figure 2a. The spectral intensity in the $\nu_\perp$ region decreases, and the peak shifts to the blue side as a result of the disruption of the β sheet. Also, the level of the random coil component between the $\nu_\perp$ and $\nu_\parallel$ modes slightly increases. The melting curves are constructed from $C^{(2)}(T)$, the second

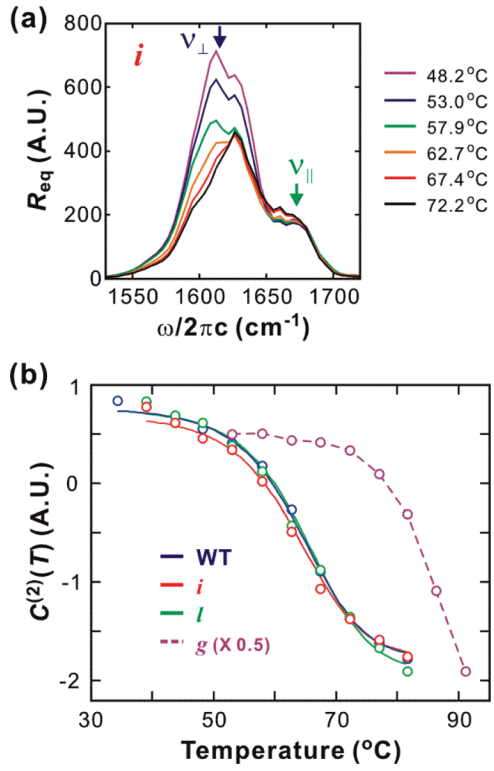

FIGURE 2: Equilibrium thermal unfolding of wild-type ubiquitin and three mutants, *i*, *l*, and *g*. (a) Temperature-dependent equilibrium DVE spectra of mutant *i*. (b) Melting curves (—) are constructed by thermodynamic fitting (two-state) to the SVD second components (○). For mutant *g*, thermodynamic analysis is not possible due to incomplete unfolding, and a dashed line is added to assist the reader.

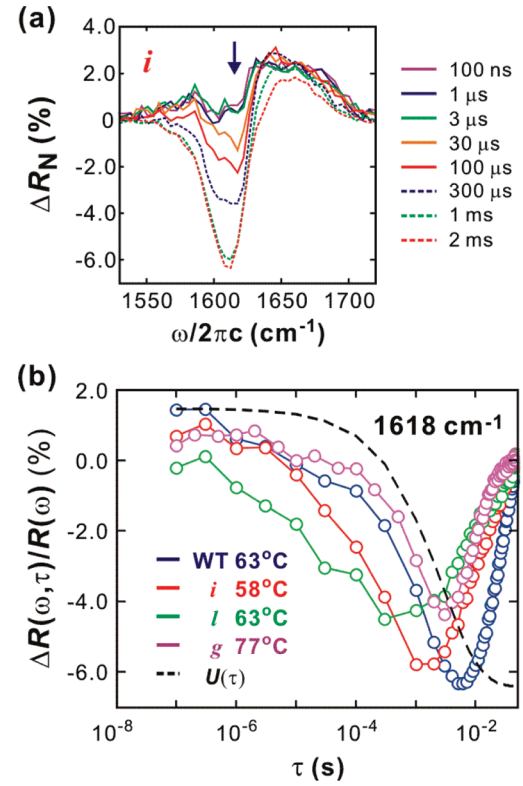

FIGURE 3: Transient thermal unfolding initiated by a T-jump. (a) Shown are transient DVE difference spectra of mutant *i* (from 57.9 to 68.2 °C). (b) Spectral change of the $\nu_\perp$ mode (1618 cm^{-1}) indicated with an arrow in panel a and temperature relaxation profile $U(\tau)$. The upturn on the millisecond time scale is due to the temperature recovery of the observation cell.

Table 1: Thermodynamic Parameters of Wild-Type and Mutant Ubiquitin

	T_m (°C)	ΔH_m (kcal/mol)	ΔS_m (cal mol^{-1} K^{-1})	ΔC_p (cal mol^{-1} K^{-1})
WT	64.0 ± 0.4	40.9 ± 1.4	121 ± 4	1300 ± 200
i	63.2 ± 0.4	39.4 ± 1.4	117 ± 4	1300[a]
l	64.9 ± 0.4	40.9 ± 1.4	121 ± 4	1300[a]

[a] Fitting was conducted with the ΔC_p fixed to the WT value.

component from singular-value decomposition (SVD) (Figure 2b). A sigmoid shape is fitted to the equations below (*44*) to yield the thermodynamic parameters summarized in Table 1

$$K = \frac{P_U}{P_F} = \exp[-\Delta G(T)/RT]$$
$$\Delta G(T) = \Delta H(T) - T\Delta S(T) \quad (1)$$
$$-\Delta S_m(T - T_m) - \frac{\Delta C_p}{2T_m}(T - T_m)^2$$

where $\Delta H = \Delta H_m + \Delta C_p(T - T_m)$, $\Delta S = \Delta S_m + \Delta C_p \ln(T/T_m)$, and ΔH and ΔS are the temperature-dependent enthalpy and entropy of unfolding, respectively. ΔH_m and ΔS_m are the enthalpy and entropy of unfolding at the melting temperature T_m (=$\Delta H_m/\Delta S_m$), respectively. Higher-order temperature terms are ignored in the Taylor expansion of ΔS. The fractional populations of the unfolded and folded state, P_U and P_F, respectively, satisfy the relation $P_U + P_F = 1$. The heat capacity change, ΔC_p, is assumed to be constant for the mutants, as a result of the large uncertainty in its determination relative to the other variables. Floating ΔC_p for all mutants resulted in unreasonable variation. Assuming that the variation of ΔC_p is smaller than the error for WT, we used the same fixed value for mutants *i* and *l*. The similar errors for other variables confirm the validity of this procedure.

The melting temperatures of WT, mutant *l*, and mutant *i* are similar. The melting curve of mutant *g* shows that thermal unfolding is not complete even at 91 °C. Therefore, thermodynamic parameters cannot be obtained from mutant *g*.

Transient Thermal Unfolding. Typical transient spectral changes from 100 ns to 2 ms are shown in Figure 3a. DVE difference spectra [$\Delta R(\omega,\tau) = R(\omega,\tau) - R_{ref}(\omega,T_i)$] are normalized by the maximum of the reference spectrum, $R_{ref}(T_i)$, obtained by the two probe pulses preceding a T-jump pulse. (Note that there are 50 probe pulses between two T-jump pulses.) At the earliest delay (100 ns), there are positive changes over the whole spectral range, which result from the increased solvent transmission of the 6 μm probe beam at the elevated temperature. A gradual signal loss in the $\nu_\perp$ region and an increase in the random coil region indicate thermal unfolding of the β sheet as seen in the equilibrium changes in Figure 2a.

Transient spectral changes in the $\nu_\perp$ region (ω = 1618 cm^{-1}) from nanosecond to millisecond time scales are plotted in Figure 3b along with the temperature relaxation profile, $U(\tau)$. The data show a variation of unfolding time scales between mutants. The spectral difference is normalized by the reference signal at the same frequency as $\Delta R(\omega,\tau)$/

$R_{ref}(\omega,T_i)$. In general, the proteins unfold over time scales from several microseconds to several milliseconds. As the temperature of the cell re-equilibrates (τ_r = 2.7 ms), the protein begins to refold before unfolding is complete. The system refolds after reaching a balanced position ($k_uP_F = k_fP_U$), where incomplete unfolding is balanced with refolding. However, the time scales of unfolding and refolding and the unfolding spectral features are different for each protein. The unfolding of the WT consists of two distinct relaxations on the microsecond and millisecond time scales. On the other hand, those two components are not clearly resolved in mutants *i* and *l*. Also, they exhibit faster unfolding than WT. Unfolding of mutant *g* occurs mostly on the millisecond time scale. The crossover to refolding kinetics at the balanced position differs by several milliseconds.

We analyzed the data before and after the balanced position separately to obtain millisecond folding−unfolding kinetics information from the latter and microsecond downhill unfolding features from the former, respectively. In addition, the time window from ~1 to 10 ms is not included in the analysis because of the complication by the temperature relaxation.

Unfolding Kinetics. We describe here the analysis methods briefly. The details for WT have been described in ref *30*. For the improvement of the signal-to-noise ratio, transient data of the $\nu_\perp$ region (1582−1651 cm^{-1}) of each mutant are extracted using SVD. Since the temperature relaxation is faster than the millisecond unfolding, the slow unfolding part is complicated by the temperature-dependent transmission change. We assume that the temperature-dependent part is a product of the temperature profile, $U(\tau)$, and the difference spectrum at the earliest delay, 100 ns, and subtract this from the DVE difference spectra prior to SVD (*30*).

$$\Delta\Delta R(\omega,\tau) = \Delta R(\omega,\tau) - U(\tau)\times\Delta R(\omega,\tau = 100\text{ ns}) \quad (2)$$

$U(\tau) = \exp[-(\tau/\tau_r)^\beta]$ (β = 0.68, and τ_r = 2.7 ms) is obtained from the transmission changes at 6 μm. Then, the relative spectral relaxation profile is constructed using the first SVD component coefficient [$C^{(1)}(\tau)$], the first component spectrum [$R^{(1)}_{SVD}$], and equilibrium difference ΔR_{eq}

$$\Delta R_{rel}(\tau) = C^{(1)}(\tau)\frac{\text{Max}|R^{(1)}_{SVD}|}{\text{Max}|\Delta R_{eq}|} \quad (3)$$

The results are shown in Figure 4 and are described below.

The most important feature of WT unfolding is the relaxation on two different time scales. The faster period occurs over several microseconds, which is close to the speed limit of protein folding (*30*) and is attributed to the barrier-free unfolding from the transition state (*26, 30*). The slow unfolding part on the millisecond time scale is an activated, barrier-crossing process. To obtain time scales, the unfolding part is fitted with a sum of stretched exponential (microseconds) and exponential (milliseconds) functions.

$$\Delta R_{rel}(\tau) = A_{\mu s}\exp[-(\tau/\tau_{\mu s})^\beta] + A_{ms}\exp(-\tau/\tau_{ms}) \quad (4)$$

where τ is the delay time ranging from 100 ns to the time when $\Delta R_{rel}(\tau)$ reaches its minimum, the balanced position. Fitting results are summarized in Table 2. Also, the relative folded population near the barrier ($P_{\mu s}/P_F$) at T_i is calculated from the relationship $P_{\mu s} = A_{\mu s}[P_F(T_i) - P_F(T_f)]$. The equilibrium population $P_F(T)$ is calculated using eq 1. $\tau_{\mu s}$ provides the stretched exponential unfolding rate constant of 1/(1.8 μs). Due to the temperature change on the millisecond time scale, the activated unfolding time ($1/k_u$) cannot be obtained from the 1−10 ms window. As a result of the time scale separation, in eq 4 we use the exponential function for the millisecond unfolding only as a guide function to help obtain exact microsecond unfolding parameters. A more careful analysis of the millisecond behavior follows.

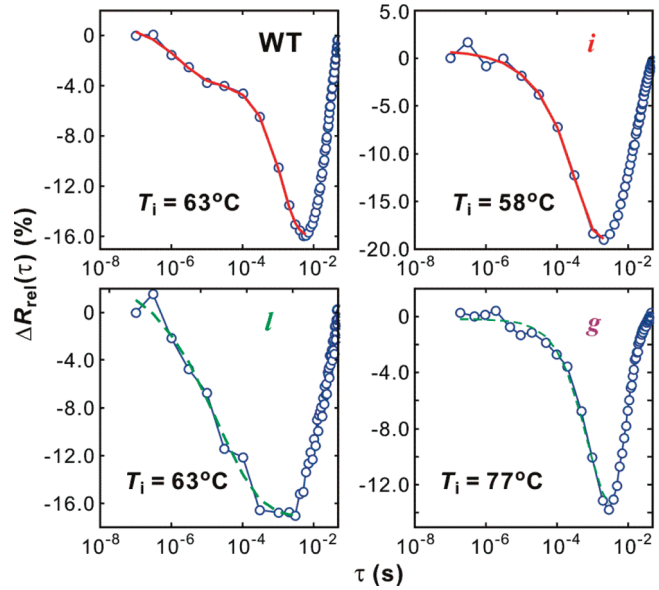

FIGURE 4: Relaxations of the $\nu_\perp$ region (1582−1651 cm^{-1}) of wild-type ubiquitin and mutants. The unfolding parts are fitted with stretched exponential + exponential (red lines) or a single stretched exponential (green dashed lines) function.

Table 2: Relaxation Parameters Obtained from the Unfolding Portion of the SVD Analysis of the $\nu_\perp$ Region (1582−1651 cm^{-1})[a]

	$T_i - T_f$ (°C)	β[b]	$\tau_{\mu s}$ (μs)[b]	$A_{\mu s}$ (%)[c]	$A_{\mu s} + A_{ms}$ (%)[c]	$P_{\mu s}/P_F$ (%)[d]
WT	62.7 − 74.3	0.62 ± 0.24	1.8 ± 0.5	4.8 ± 0.6	17.0 ± 0.6	3.8 ± 0.5
i	53.0 − 63.3	0.61 ± 0.33	9.3 ± 4	4.3 ± 1.3	13.2 ± 1.5	1.8 ± 0.6
	57.9 − 68.2	0.57 ± 0.95	45.3 ± 24.9	6.3 ± 3.8	19.8 ± 4.8	3.8 ± 2.3
	62.7 − 74.5	0.83 ± 0.44	20.7 ± 28.6	11.9 ± 6.8	22.6 ± 11.9	9.4 ± 5.4
l	57.9 − 67.3	0.29 ± 0.07	76 ± 56	8.9 ± 1.3	–	3.2 ± 0.5
	62.7 − 71.9	0.38 ± 0.09	21 ± 10	20.5 ± 2.5	–	7.2 ± 0.9
g	72.2 − 83.8	0.95 ± 0.11	646 ± 57	9.8 ± 0.2	–	–
	77.0 − 88.6	0.87 ± 0.08	725 ± 60	13.6 ± 0.2	–	–

[a] Unfolding traces of WT and mutant *i* are fit to the sum of a stretched exponential (microsecond part) and an exponential (millisecond part) function {$A_{\mu s}\exp[-(\tau/\tau_{\mu s})^\beta] + A_{ms}\exp(-\tau/\tau_{ms})$}, while the whole unfolding traces of mutants *l* and *g* are fit to a stretched exponential function. [b] β and $\tau_{\mu s}$ are the stretched exponential parameters for the microsecond relaxation part. [c] $A_{\mu s}$ and A_{ms} are the relative amplitudes of the microsecond and millisecond relaxation, respectively, compared to the expected, equilibrium-determined change to the final temperature of the T-jump. [d] $P_{\mu s}/P_F$ is the relative amplitude change during the microsecond relaxation to the folded population at the initial temperature.

Compared to that of WT, the barrierless unfolding of mutant *i* is slower (9−45 μs) but its amplitude is bigger than that of WT at similar temperatures (Table 2). The unfolding transients of mutants *l* and *g* are fit to a single stretched exponential because either the microsecond component or the millisecond component is small. Unfolding of mutant *l* is highly heterogeneous (β < 0.4), whereas the high β value of mutant *g* indicates that the fast barrierless unfolding is minimal. This indicates that the stabilization of strands III

Table 3: Parameters for Refolding Kinetics Obtained from the Refolding Portion of the Transients after Temperature Re-Equilibration

	T (°C)	τ_r (ms)	k_f (s^{-1})	k_u (s^{-1})
WT	62.7	16.7 ± 0.6	33 ± 2	27 ± 1
i	53.0	14.9 ± 0.4	55 ± 2	12 ± 1
	57.9	14.1 ± 0.3	50 ± 2	21 ± 1
	62.7	11.8 ± 0.4	44 ± 2	41 ± 2
l	57.9	18.9 ± 1.1	40 ± 2	13 ± 1
	62.7	17.3 ± 1.0	33 ± 2	23 ± 2
g	72.2	8.3 ± 0.2	−	−
	77.0	8.4 ± 0.1	−	−

and V by cross-linking removes downhill unfolding relaxation present in WT. Such an observation is expected if disorder of the III−V strand contacts determines the position of the WT transition state and leads to the microsecond downhill unfolding population.

The overall fitting errors of the microsecond time scale parameters are not small enough to distinguish a time scale of 1−2 μs and describe changes in the free energy surface quantitatively. However, these microsecond changes are real and independent of the temperature relaxation given that spectral changes on the 1−100 μs time scale are at least 1 order of magnitude faster than that of temperature relaxation. In our previous experiments on *N*-methylacetamide (NMA) (*40*) containing only one amide oscillator group and on ubiquitin at 25 °C (*30*), where no structural change is expected except the ultrafast solvation dynamics, the spectral responses follow the temperature relaxation profile, which exhibit very little change from 100 ns to 100 μs.

Refolding Kinetics. Although the determination of the millisecond unfolding kinetics cannot be made accurately, we can still obtain the refolding kinetics after the temperature re-equilibrates. The temperature after 10 ms is approximately same as T_i (<1 °C difference), and the folding and unfolding rates are essentially constant. In this case, an exponential fit of the refolding part gives the relaxation rate that is the sum of the folding and unfolding rates ($k_r = k_f + k_u$). Using this value and the equilibrium constant ($K = k_u/k_f$) obtained from the equilibrium measurement, folding and unfolding rates can be obtained. These values are summarized in Table 3.

The relaxation rate (k_r) of mutant *g* is the fastest. This increase may be due to the experiment being performed at the elevated melting point where solvent viscosity is decreased and chain diffusion is faster. The barrier to unfolding of mutant *i* is lower than that of WT as seen from the faster unfolding rate and the higher unfolding population near the barrier. On the other hand, the refolding relaxation of mutant *l* is slower than those of WT and mutant *i*, indicating a higher barrier, which is contradictory to fast microsecond unfolding of mutant *l*. Because the melting temperatures of mutant *l* and WT are very close, millisecond unfolding (barrier crossing) of mutant *l* will be slower than that of WT as its slower refolding. As explained earlier, the fact that temperature re-equilibration ($\tau_r = 2.7$ ms) is faster than barrier-crossing unfolding makes thermal unfolding incomplete, and slower unfolding of mutant *l* results in the smaller millisecond unfolding amplitude. In fact, the time scale and amplitude obtained from the global fit (a single stretched exponential) of mutant *l* unfolding (Table 2) are similar to those of microsecond unfolding of mutant *i*. Therefore, the unfolding phase of mutant *l* is dominated by a barrierless process, and the amount of millisecond unfolding is very small due to the higher barrier.

DISCUSSION

Unfolding Mechanism and Origin of Microsecond Unfolding. A temperature-dependent barrier shift illustrated in Figure 1c is the basis of our interpretation of unfolding on the two distinct time scales: a microsecond downhill process and a millisecond barrier crossing. However, this one-dimensional picture does not provide any structural information during unfolding. In earlier work, a two-dimensional free energy surface of thermal unfolding of ubiquitin was proposed on the basis of the observation of noncoincident relaxation of the $\nu_\perp$ and $\nu_\parallel$ modes on the microsecond time scale (*26*). This free energy surface is illustrated in Figure 5a for WT. Signal changes of these two vibrational modes report on the reduction in size of the β sheet followed by disappearance of the β hairpin, which indicates a sequential unfolding of the β sheet. This observation and the numerous experimental and theoretical results supporting the stability of the β hairpin consisting of strands I and II (*18*−*24*) suggest a free energy surface consisting of two reaction coordinates: the number of native contacts between the stable β strands (I and II) and between the less stable β strands (III−V). The temperature dependence of this free energy surface of ubiquitin unfolding has been investigated by statistical mechanical calculations (*29*).

In the proposed free energy surface, the transition state is characterized by fully folded stable strands I and II and partially folded strands III and V, consistent with the extended transition state identified using ψ value analysis (*7, 8*). With a T-jump, the transition state moves toward the folded well along the coordinate *n*(III,IV,V) and the population positioned around the barrier unfolds in a downhill manner, first along *n*(III,IV,V) (unfolding of strands III−V) and then along *n*(I,II) (unfolding of the remaining β hairpin). In this picture, therefore, the amplitude of this fast phase will be dependent on the stability of strands III−V. This is consistent with the increased (decreased) amplitude of the microsecond component for mutant *i* (*g*) upon destabilization (stabilization) of strands III−V. In ref *7*, the ψ values for mutants *l* and *i* were unity and near zero, respectively. For mutant *g*, the $\phi^{\text{cross-link}}$ value was fractional while the ψ value for a bi-His analogue was near unity (*31*). These results indicate that in the transition state, the C-terminal portion of the helix is nativelike while the strands III and V are associated in a near-native arrangement but strands III and IV are not associated. However, this transition state cannot explain the amplitude variation of the microsecond unfolding in mutants *i* and *g* in thermal unfolding. Therefore, we conclude that both strands III and V are partially folded in the transition state at high temperatures and low pH.

Intermediate State. The presence of the intermediate state in ubiquitin folding has long been under debate because of the controversial results from similar experiments (*45*−*48*). In stopped-flow measurements, the rollover at low denaturant concentrations in the chevron plot is used to argue for an early intermediate state. For ubiquitin, the appearance of this rollover depends on experimental conditions such as the concentration of the protein and the stabilizing salt and temperature (*47*). Sosnick and co-workers have pointed out

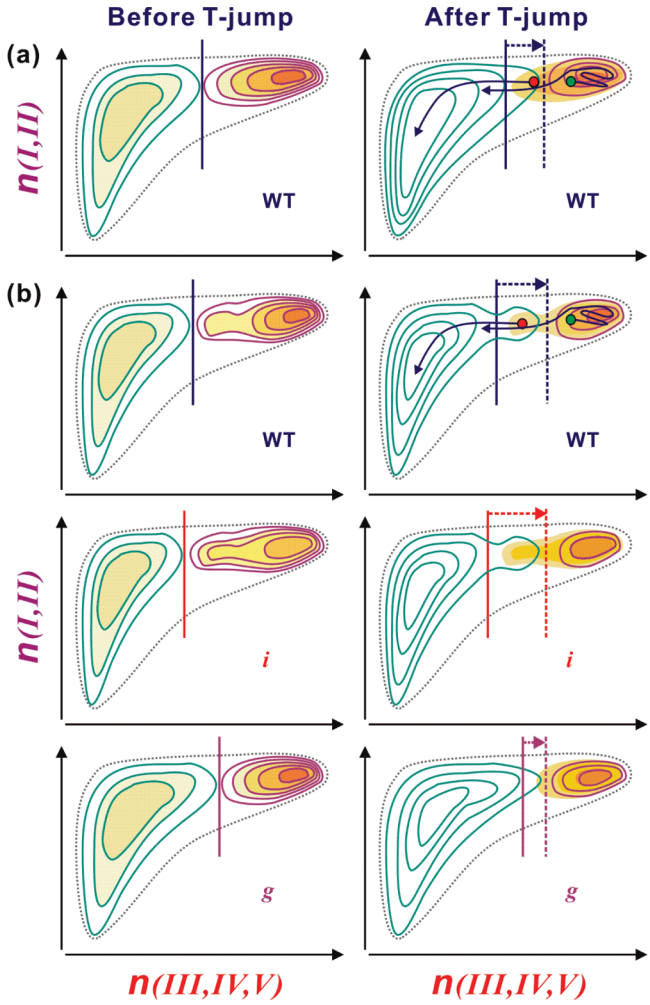

FIGURE 5: Proposed free energy surfaces. Vertical and horizontal axes indicate the number of native contacts between stable strands I and II [n(I,II)] and among less stable strands III−V [n(III,IV,V)], respectively. Vertical solid and vertical dashed lines indicate the barrier position before and after the T-jump, respectively. (a) Free energy surfaces for WT in the absence of the intermediate state. The barrier shift by a rapid temperature jump toward the folded well induces downhill unfolding of the folded population located in the unfolded side of the new barrier (red dot), which is followed by millisecond unfolding from the folded well (green dot) across the barrier. (b) Free energy surfaces in the presence of the intermediate state where strands III and V are partially folded. For WT, the intermediate state belongs to the folded side before the temperature jump and the barrier is formed between the intermediate state and the unfolded state. At higher temperatures after the T-jump, the intermediate state belongs to the unfolded side with a negligible barrier and the major barrier is formed between the intermediate state and the folded state. In this case, the partially unfolded protein at the intermediate state unfolds in a downhill manner on the microsecond time scale, which is also followed by millisecond unfolding. For mutant *i*, the unfolding features are similar to those of WT, but the intermediate state is more populated due to the destabilization of strands III and IV in the folded state. The more populated intermediate state results in larger-amplitude microsecond unfolding. In the case of mutant *g*, the intermediate state almost disappears because of the stabilization of strands III and V, which removes the barrier between the intermediate state and the folded state at all temperatures.

that this rollover can result from an artifact in fitting when the relaxation rate is close to the dead time of the apparatus and is affected by the burst phase (*45, 46*). In addition, results are also affected by the method of probing and the location of the chromophore. Recently, folding of different parts of ubiquitin has been monitored by multiple tryptophan substitutions, which is interpreted as the presence of a late but partially misfolded intermediate state (*49*).

In a previous temperature-dependent thermal unfolding study of WT, we noted that the microsecond unfolding population is much larger than the amount deduced from the barrier height of 7 kcal/mol (*30*), which may indicate the presence of the intermediate state on the native side of the barrier in the thermal unfolding case as well. In Figure 5b, we illustrate an alternate free energy surface in the presence of the intermediate state, consistent with the present experiments and ψ analysis. An on-pathway intermediate located between the folded and unfolded state has strands III and V partially disordered, while strand IV is unfolded. At low temperatures, the intermediate state is the part of the folded well and the rate-limiting folding barrier is located between the intermediate state and the unfolded state. The barrier between the intermediate state and the folded state is small or negligible. The microsecond unfolding also originates from a barrier shift toward the folded well with a T-jump. However, in this case, the presence of the intermediate state can lead to a larger barrier shift that positions the major folding barrier between the intermediate and the folded state (Figure 5b). Also, the barrier between the intermediate and unfolded state becomes small or negligible, which induces a barrierless unfolding with an amplitude larger than that expected in the two-state system.

For mutant *i*, the situation is similar but the intermediate state is more populated because the energy difference between the intermediate state and the folded state is smaller than that of WT due to the destabilization of strands III and IV. The more populated intermediate state results in the larger amplitude of microsecond unfolding. On the other hand, the stabilization of strands III and V by cross-linking removes the barrier between the intermediate state and the folded state at all temperatures, resulting in negligible microsecond unfolding of mutant *g* (Figure 5b).

CONCLUSIONS

The transition state of thermal unfolding of ubiquitin has been investigated by a combination of site-specific mutations and a laser T-jump experiment probed by DVE spectroscopy. We compare the amplitudes of the nonexponential microsecond unfolding relaxation between mutants and WT, which reflects population changes near the transition state. The destabilization of β strands III and IV (mutant *i*) induces an increased microsecond unfolding amplitude, whereas the stabilization of contacts between strands III and V (mutant *g*) results in its decrease. On the basis of these observations, we conclude that the transition state of WT is extended to strands V and III at the thermal melting temperature. Also, the observation of a microsecond unfolding amplitude larger than that expected from two-state kinetics supports the presence of an intermediate state. These observations were discussed in terms of a modified two-dimensional free energy surface. In addition, several observations in mutant *l* such as the origin of faster unfolding in spite of a higher barrier compared to mutant *i* and WT remain unanswered, and more thorough mutation studies are required for quantitative analyses.

REFERENCES

1. Creighton, T. E. (1990) Protein folding. *Biochem. J. 270*, 1–16.

2. Fersht, A. R. (1997) Nucleation mechanisms in protein folding. *Curr. Opin. Struct. Biol. 7*, 3–9.
3. Jackson, S. E. (1998) How do small single-domain proteins fold? *Folding Des. 3*, R81−R91.
4. Fersht, A. R., and Sato, S. (2004) ϕ-value analysis and the nature of protein-folding transition states. *Proc. Natl. Acad. Sci. U.S.A. 101*, 7976–7981.
5. Pain, R. H. (2000) *Mechanisms of protein folding*, 2nd ed., Oxford University Press, Oxford, U.K.
6. Krantz, B. A., and Sosnick, T. R. (2001) Engineered metal binding sites map the heterogeneous folding landscape of a coiled coil. *Nat. Struct. Biol. 8*, 1042–1047.
7. Krantz, B. A., Dothager, R. S., and Sosnick, T. R. (2004) Discerning the structure and energy of multiple transition states in protein folding using ψ-analysis. *J. Mol. Biol. 337*, 463–475.
8. Sosnick, T. R., Dothager, R. S., and Krantz, B. A. (2004) Differences in the folding transition state of ubiquitin indicated by ϕ and ψ analyses. *Proc. Natl. Acad. Sci. U.S.A. 101*, 17377–17382.
9. Sabelko, J., Ervin, J., and Gruebele, M. (1999) Observation of strange kinetics in protein folding. *Proc. Natl. Acad. Sci. U.S.A. 96*, 6031–6036.
10. Yang, W. Y., and Gruebele, M. (2003) Folding at the speed limit. *Nature 423*, 193–197.
11. Kubelka, J., Hofrichter, J., and Eaton, W. A. (2004) The protein folding 'speed limit'. *Curr. Opin. Struct. Biol. 14*, 76–88.
12. Garcia-Mira, M. M., Sadqi, M., Fischer, N., Sanchez-Ruiz, J. M., and Muñoz, V. (2002) Experimental Identification of Downhill Protein Folding. *Science 298*, 2191–2195.
13. Sadqi, M., Fushman, D., and Muñoz, V. (2006) Atom-by-atom analysis of global downhill protein folding. *Nature 442*, 317–321.
14. Naganathan, A. N., Doshi, U., and Muñoz, V. (2007) Protein folding kinetics: Barrier effects in chemical and thermal denaturation experiments. *J. Am. Chem. Soc. 129*, 5673–5682.
15. Ferguson, N., Sharpe, T. D., Johnson, C. M., Schartau, P. J., and Fersht, A. R. (2007) Analysis of 'downhill' protein folding. *Nature 445*, E14−E15.
16. Zhou, Z., and Bai, Y. (2007) Analysis of protein-folding cooperativity. *Nature 445*, E16−E17.
17. Sadqi, M., Fushman, D., and Muñoz, V. (2007) Sadqi et al. reply. *Nature 445*, E17−E18.
18. Cox, J. P. L., Evans, P. A., Packman, L. C., Williams, D. H., and Woolfson, D. N. (1993) Dissecting the structure of a partially folded protein circular dichroism and nuclear magnetic resonance studies of peptides from ubiquitin. *J. Mol. Biol. 234*, 483–492.
19. Jourdan, M., and Searle, M. S. (2000) Cooperative assembly of a nativelike ubiquitin structure through peptide fragment complexation: Energetics of peptide association and folding. *Biochemistry 39*, 12355–12364.
20. Harding, M. M., Williams, D. H., and Woolfson, D. N. (1991) Characterization of a partially denatured state of a protein by two-dimensional NMR: Reduction of the hydrophobic interactions in ubiquitin. *Biochemistry 30*, 3120–3128.
21. Stockman, B. J., Euvrard, A., and Scahill, T. A. (1993) Heteronuclear three-dimensional NMR spectroscopy of a partially denatured protein: The A-state of human ubiquitin. *J. Biomol. NMR 3*, 285–296.
22. Cordier, F., and Grzesiek, S. (2004) Quantitative comparison of the hydrogen bond network of A-state and native ubiquitin by hydrogen bond scalar couplings. *Biochemistry 43*, 11295–11301.
23. Went, H. M., and Jackson, S. E. (2005) Ubiquitin folds through a highly polarized transition state. *Protein Eng. Des. Sel. 18*, 229–237.
24. Marianayagam, N. J., and Jackson, S. E. (2004) The folding pathway of ubiquitin from all-atom molecular dynamics simulations. *Biophys. Chem. 111*, 159–171.
25. Hammond, G. S. (1955) A correlation of reaction rates. *J. Am. Chem. Soc. 77*, 334–338.
26. Chung, H. S., Khalil, M., Smith, A. W., Ganim, Z., and Tokmakoff, A. (2005) Conformational changes during the nanosecond to millisecond unfolding of ubiquitin. *Proc. Natl. Acad. Sci. U.S.A. 102*, 612–617.
27. Chung, H. S., Ganim, Z., Jones, K. C., and Tokmakoff, A. (2007) Transient 2D IR spectroscopy of ubiquitin unfolding dynamics. *Proc. Natl. Acad. Sci. U.S.A. 104*, 14237–14242.
28. Alonso, D. O. V., and Daggett, V. (1998) Molecular dynamics simulations of hydrophobic collapse of ubiquitin. *Protein Sci. 7*, 860–874.
29. Chung, H. S., and Tokmakoff, A. (2008) Temperature-dependent downhill unfolding of ubiquitin. II. Modeling the free energy surface. *Proteins: Struct., Funct., Bioinf. 72*, 488–497.
30. Chung, H. S., and Tokmakoff, A. (2008) Temperature-dependent downhill unfolding of ubiquitin. I. Nanosecond-to-millisecond resolved nonlinear infrared spectroscopy. *Proteins: Struct., Funct., Bioinf. 72*, 474–487.
31. Shandiz, A. T., Capraro, B. R., and Sosnick, T. R. (2007) Intramolecular cross-linking evaluated as a structural probe of the protein folding transition state. *Biochemistry 46*, 13711–13719.
32. Ibarra-Molero, B., Loladze, V. V., Makhatadze, G. I., and Sanchez-Ruiz, J. M. (1999) Thermal versus guanidine-induced unfolding of ubiquitin. An analysis in terms of the contributions from charge-charge interactions to protein stability. *Biochemistry 38*, 8138–8149.
33. Colley, C. S., Clark, I. P., Griffiths-Jones, S. R., George, M. W., and Searle, M. S. (2000) Steady state and time-resolved IR spectroscopy of the native and unfolded states of bovine ubiquitin: Protein stability and temperature-jump kinetic measurements of protein folding at low pH. *Chem. Commun.,* 1493–1494.
34. Khorasanizadeh, S., Peters, I. D., Butt, T. R., and Roder, H. (1993) Folding and stability of a tryptophan-containing mutant of ubiquitin. *Biochemistry 32*, 7054–7063.
35. Krimm, S., and Bandekar, J. (1986) Vibrational spectroscopy and conformation of peptides, polypeptides and proteins. *Adv. Protein Chem. 38*, 181–364.
36. Cheatum, C. M., Tokmakoff, A., and Knoester, J. (2004) Signatures of β-sheet secondary structures in linear and two-dimensional infrared spectroscopy. *J. Chem. Phys. 120*, 8201–8215.
37. Byler, D. M., and Susi, H. (1986) Examination of the secondary structure of proteins by deconvolved FTIR spectra. *Biopolymers 25*, 469–487.
38. Khalil, M., Demirdoven, N., and Tokmakoff, A. (2003) Coherent 2D IR Spectroscopy: Molecular Structure and Dynamics in Solution. *J. Phys. Chem. A 107*, 5258–5279.
39. Chung, H. S., Khalil, M., and Tokmakoff, A. (2004) Nonlinear infrared spectroscopy of protein conformational change during thermal unfolding. *J. Phys. Chem. B 108*, 15332–15343.
40. Chung, H. S., Khalil, M., Smith, A. W., and Tokmakoff, A. (2007) A transient 2D IR spectrometer for probing nanosecond temperature-jump kinetics. *Rev. Sci. Instrum. 78*, 063101.
41. Smith, A. W., and Tokmakoff, A. (2007) Probing local structural events in β-hairpin unfolding with transient nonlinear infrared spectroscopy. *Angew. Chem., Int. Ed. 46*, 7984–7987.
42. Eaton, W. A., Muñoz, V., Thompson, P. A., Henry, E. R., and Hofrichter, J. (1998) Kinetics and dynamics of loops, α-helices, β-hairpins, and fast-folding proteins. *Acc. Chem. Res. 31*, 745–753.
43. Callender, R. H., Dyer, R. B., Gilmanshin, R., and Woodruff, W. H. (1998) Fast events in protein folding: The time evolution of primary processes. *Annu. Rev. Phys. Chem. 49*, 173–202.
44. Makhatadze, G. I., and Privalov, P. L. (1995) Energetics of protein structure. *Adv. Protein Chem. 47*, 307–425.
45. Krantz, B. A., and Sosnick, T. R. (2000) Distinguishing between two-state and three-state models for ubiquitin folding. *Biochemistry 39*, 11696–11701.
46. Krantz, B. A., Mayne, L., Rumbley, J., Englander, S. W., and Sosnick, T. R. (2002) Fast and slow intermediate accumulation and the initial barrier mechanism in protein folding. *J. Mol. Biol. 324*, 359–371.
47. Went, H. M., Benitez-Cardoza, C. G., and Jackson, S. E. (2004) Is an intermediate state populated on the folding pathway of ubiquitin? *FEBS Lett. 567*, 333–338.
48. Roder, H., Maki, K., and Cheng, H. (2006) Early events in protein folding explored by rapid mixing methods. *Chem. Rev. 106*, 1836–1861.
49. Vallée-Bélisle, A., and Michnick, S. W. (2007) Multiple tryptophan probes reveal that ubiquitin folds via a late misfolded intermediate. *J. Mol. Biol. 374*, 791–805.
50. Vijay-Kumar, S., Bugg, C. E., and Cook, W. J. (1987) Structure of ubiquitin refined at 1.8 Å resolution. *J. Mol. Biol. 194*, 531–544.

BI801603E